Tetrahedron: *Asymmetry* xxx (2015) xxx–xxx

Contents lists available at ScienceDirect

Tetrahedron: *Asymmetry*

journal homepage: www.elsevier.com/locate/tetasy

Aza and oxo Diels–Alder reactions using *cis*-cyclohexadienediols of microbial origin: chemoenzymatic preparation of synthetically valuable heterocyclic scaffolds

Mariana Pazos [a], Sebastián Martínez [b], María Agustina Vila [a], Paola Rodríguez [a], Nicolás Veiga [b], Gustavo Seoane [a], Ignacio Carrera [a,*]

[a] *Laboratorio de Química Orgánica, Departamento de Química Orgánica, Facultad de Química—Universidad de la República, General Flores 2124, 11800 Montevideo, Uruguay*
[b] *Cátedra de Química Inorgánica, Departamento Estrella Campos, Facultad de Química—Universidad de la República, General Flores 2124, 11800 Montevideo, Uruguay*

ARTICLE INFO

Article history:
Received 6 October 2015
Accepted 21 October 2015
Available online xxxx

ABSTRACT

Aza and oxo Diels–Alder reactions using enantiopure *cis*-cyclohexadienediols were studied. These dienediols were obtained from the biotransformation of monosubstituted arenes using bacterial dioxygenases (toluene and benzoate dioxygenases). Ethyl glyoxylate and its *N*-tosyl imine were used as dienophiles to afford the corresponding hetero Diels–Alder bicyclic adducts with excellent regio- and stereoselectivities. Quantum chemical calculations at the B3LYP/6-31+G(d,p) level of theory were performed to rationalize the observed selectivities especially the stereochemical aspects of the cycloadditions. The synthetic importance of these adducts is highlighted for the preparation of enantiopure 2,2,3,4,5,6-hexasubstituted piperidine and tetrahydropyran from toluene.

1. Introduction

Enantiopure *cis*-cyclohexadienediols have been extensively used as starting materials for the enantioselective organic synthesis of complex natural products.[1] These compounds can be prepared from the corresponding arenes by enzymatic dihydroxylation using bacterial dioxygenases since no other efficient chemical method for their production at a preparative scale is known.[2] The biotransformation is carried out using whole cells as the biocatalyst to overcome the need of recycling co-factors as well as to avoid the difficult procedures of enzyme isolation and purification.[1f] The most commonly used biocatalyst on a preparative scale for the production of *cis*-cyclohexadienediols of type **1** is the recombinant *Escherichia coli* JM109 (pDTG601), which expresses the toluene dioxygenase enzymatic complex (Scheme 1).[3] For the production of *cis*-cyclohexadienediols of type **2** the microorganism *Ralstonia eutropha* B9, that expresses a benzoate dioxygenase, has recently been used for organic synthesis applications.[4] The useful array of functional groups present in **1** and **2** allows the use of regio- and stereocontrolled organic transformations resulting in short and efficient synthetic schemes.[1f,4a]

These systems have been extensively used as the 4π-component in diastereofacially selective Diels–Alder cycloadditions to achieve the preparation of several substituted bicyclo[2.2.2]octenes (Scheme 2). Many examples have been reported for this type of intermolecular cycloadditions using diols of type **1** and several dienophiles such as: triazolinediones,[5] acetylenes,[5b,6] *N*-substituted maleimides,[6,7] maleic anhydride,[7b,8] benzyne,[9] benzo- and naphthoquinones,[9] nitrosyl derivatives,[5b,6,10] singlet oxygen,[11] α-chloroacrylonitriles,[12] and cyclopentenones.[13] The exploitation of diols of type **2** as dienes for these cycloadditions is found in the literature with nitrosyl groups,[4c,j,14] alkenes,[4f,h] singlet oxygen,[4a,15] and urazole dienophiles.[4d,j]

Herein we have studied the aza and oxo Diels–Alder cycloadditions of isopropylidene protected *cis*-cyclohexadienediols using ethyl glyoxylate and its *N*-tosyl imine as dienophiles. These dienophiles have been used for heterocycle preparation through a hetero Diels–Alder methodology,[16] but to our knowledge, there is no previous report of their use with *cis*-cyclohexadienediols to produce the expected bicyclo[2.2.2]octenes. These heterocyclic scaffolds present a high synthetic potential for natural product synthesis, especially for the preparation of enantiopure polysubstituted piperidines and tetrahydropyrans. Polysubstituted piperidine and tetrahydropyran heterocycles are important structural motifs found in a wide range of biologically active natural products, and are often key pharmacophores in drug design.[17] Previous reports

* Corresponding author. Tel.: +598 29247881.
E-mail address: icarrera@fq.edu.uy (I. Carrera).

http://dx.doi.org/10.1016/j.tetasy.2015.10.015
0957-4166/

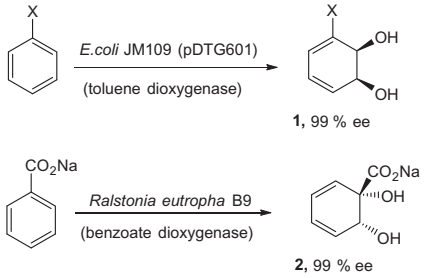

Scheme 1. Production of *cis*-cyclohexadiendiols of type **1** and **2** using bacterial dioxygenases.

have used *cis*-cyclohexadienediols as precursors of polysubstituted heterocycles using different synthetic methodologies resulting in multi step procedures.[4b,18] Using the above mentioned methodology we herein report a chemoenzymatic procedure to transform toluene into an enantiopure polysubstituted piperidine and tetrahydropyran in a rapid and efficient fashion.

2. Results and discussion

2.1. Experimental results

cis-Cyclohexadienediols of type **1** were produced by the biotransformation of monosubstituted arenes with the recombinant microorganism *E. coli* JM109 (pDTG601) using a slight modification of a previous bi-phasic procedure published by our group (see Section 4).[3b] Biotransformation yields in g/L of culture broth are shown in Scheme 3a for each substrate used. Dienediols of type **1** were protected as the isopropylidene ketals **3** with excellent yields using previously reported standard conditions and were subjected to hetero Diels–Alder cycloadditions with ethyl glyoxylate or its *N*-tosylimine. *cis*-Cyclohexadienediols of type **2** were prepared by biotransformation of sodium benzoate by *Ralstonia eutropha* B9 using a modification of the procedure published by Hudlicky et al. (Scheme 3b).[4b] The protection of **2** using dimethoxypropane for the diol moiety and diazomethane for carboxylic acid esterification afforded compound **4**, which was subjected to the mentioned hetero Diels–Alder cycloadditions.

Ethyl glyoxylate *N*-tosyl imine **5** was prepared according to the procedure described by Le Goffic et al. using ethyl glyoxylate and *p*-toluenesulphonylisothiocyanate, and used in situ without further purification (see Section 4).[19] A first attempt to perform the imino Diels–Alder reaction on substrate **1a** afforded the desired isoquinuclidines **6**, as a 75:25 mixture of diastereomers in 23% yield (Scheme 4a). Structural analysis by NMR showed complete regioselectivity for the process, which is in agreement with the charge distribution and electronic features of the reactants (see computational results below). The facial selectivity for the dienophile addition, exclusively on the less hindered face of the diene (*anti* to the bulky isopropylidene group), was proposed according to previous reports of Diels–Alder reactions on *cis*-cyclohexadienediols. The major diastereomer was identified as the *exo* carboxyethyl adduct by NOE experiments on **6** (Scheme 4b). The preference for the *exo* addition product in Diels–Alder reactions using imines containing both *N*-sulfonyl and *C*-acyl groups is already well known.[16a,20] The whole *exo* stereochemistry assignment for **6** was further confirmed by the transformation of adduct **6** into the corresponding piperidine followed by *J*-coupling analysis (vide infra, Scheme 7).

In addition to the described isoquinuclidines, the oxygenated bicyclo[2.2.2]octane **7** was obtained in 11% yield as a 91:9

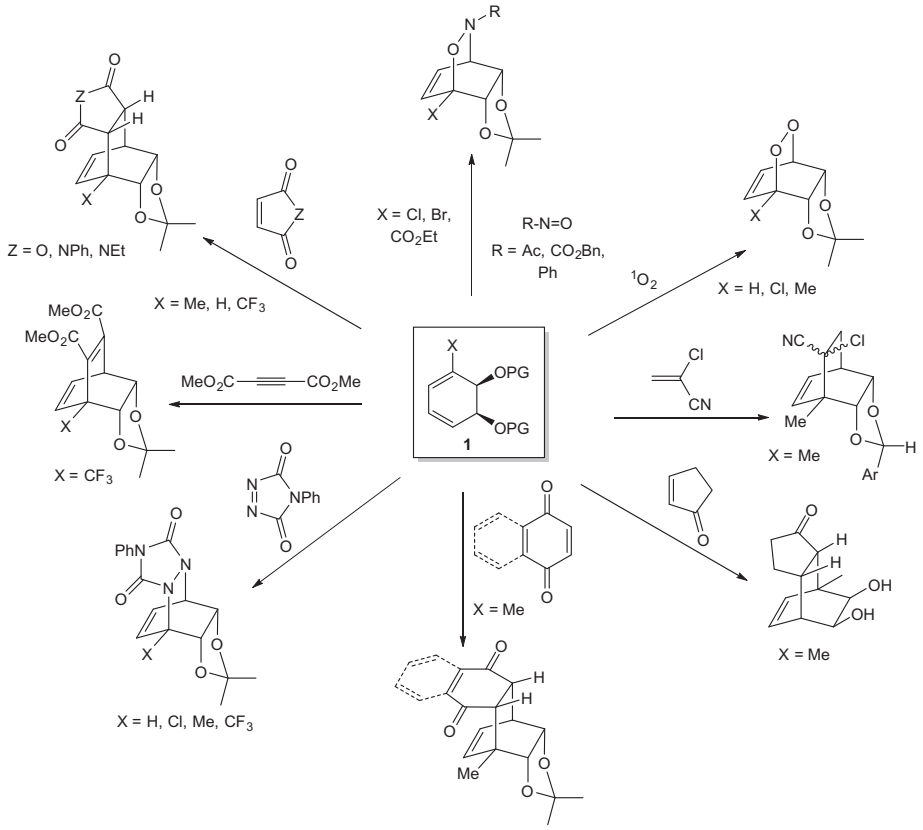

Scheme 2. Intermolecular [4 + 2] cycloadditions in *cis*-cyclohexadienediols of type **1** using different dienophiles. PG = protecting group.

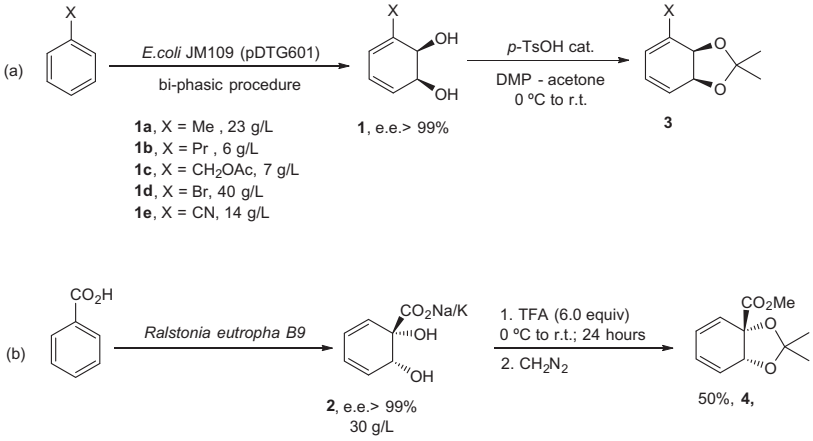

Scheme 3. (a) Arenes biotransformation using *E. coli* JM109 (pDTG601) in a bi-phasic procedure and the preparation of isopropylidene derivatives **3**. (b) Biotransformation of benzoic acid using *Ralstonia eutropha* B9 and the preparation of protected diol **4.**

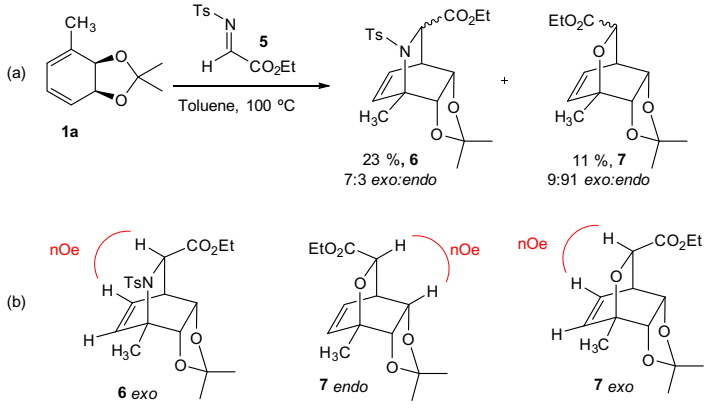

Scheme 4. (a) Imino Diels–Alder reaction of ethyl glyoxylate *N*-tosyl imine **5** and diene **1a**. (b) Diastereomer assignment by key NOE correlations.

endo/*exo* mixture of epimers. These products could arise from the reaction of diene **1a** with ethyl glyoxylate present in the reaction media as a decomposition product of the *N*-tosylimine **5** or as residual starting material of its formation. Key NOE correlations (Scheme 4a) allowed the stereochemical assignment of the *endo* and *exo* isomers. In addition, the NOE correlation found for *endo*-**7** shows that the addition of the dienophile occurred *anti* to the bulky isopropylidene group. This could be extrapolated for the *exo* isomer, which showed a similar *J* coupling pattern in the ^{1}H NMR spectra (see compound characterization in Section 4). In this case, the *endo* isomer was the major product of the reaction as expected for this type of cycloaddition.

In order to obtain a useful reaction for synthetic purposes, the optimization of the formation of isoquinuclidine **6** was carried out (Table 1). A screening of solvents (Table 1, entries 1–5) revealed that toluene was the best choice to obtain isoquinuclidines **6** with lower amounts of bicycles **7**. Different concentrations and imine equivalents were tested and the best conditions found were 0.5 M **1a** in toluene and 1.5 equivalents of *N*-tosylimine **5** at reflux**,** to produce isoquinuclidines **6** in 66% yield (Table 1, entry 7). Lewis acid catalysis [$BF_3{\cdot}OEt_2$ and $Yb(OTf)_3$] was not successful since aromatization of the starting *cis*-cyclohexadienediol took place.

The optimized conditions were used to study the reaction scope for the Diels–Alder reaction using *N*-tosylimine **5** and ethyl glyoxylate to produce the already mentioned oxygenated derivatives on different *cis*-cyclohexadienediols. For diols of type **1**, R groups with different sizes and electronic content were tested for both transformations (Scheme 5). In the case of the oxo Diels–Alder reaction, we found that when R = Me, an excellent yield of 88% for **7** was obtained, which decreased as the size of the alkyl R substituent increased (Scheme 5a). This could be explained by the increasing steric hindrance in the diene that precludes the dienophile access. Regarding the stereoselectivity of the cycloaddition, the *exo* isomer was only found in trace amounts for compound **7**, while bicycles **8** and **9** were characterized as a single *endo* diastereomer. For the aza Diels–Alder reaction, the same trend in the reactions yields for alkyl R substituents was found, although the values were significantly lower in all cases. According to these results it seems that *cis*-cyclohexadienediols are less reactive toward imine **5** than to ethyl glyoxylate for the studied cycloadditions. Thus, the only substrate useful for the preparation of the desired isoquinuclidines for synthetic purposes was found to be the *cis*-cyclohexadienediol **1a**. In all the aforementioned cases for the aza Diels–Alder reactions, *exo*/*endo* mixtures of diastereomers were found (Scheme 5a).

cis-Cyclohexadienediols with bromo and cyano groups were tested as electron withdrawing substituents for the diene system (Scheme 5b). In both cases the only products obtained were **12** and **13**, which corresponds to the already well known Diels–Alder dimerization for these systems.[21] This shows that *cis*-cyclohexadienediols with electron withdrawing groups work better as dienophiles than ethyl glyoxylate or its *N*-tosyl imine under these conditions.

We next studied these reactions on substrate **4** where the diene has no R substituents and the asymmetry of the system is given by

Table 1
Imino Diels–Alder optimization of diene **1a**

Entry	Solvent	**1a** (mol/L)	Lewis Acid	Imine **5** (equiv)	Time	Temp (°C)	**6** (%), *exo*/*endo*	**7** (%)
1	Toluene	0.10	—	1.5	8	100[a]	23, 75:25	11
2	MeCN	0.10	—	1.5	8	100[a]	17, 66:34	15
3	DCE	0.10	—	1.5	8	100[a]	26, 74:16	16
4	THF	0.10	—	1.5	8	100[a]	—	36
5	MeOH	0.10	—	1.5	8	100[a]	Aromatization products	
6	Toluene	0.25	—	1.5	4	110	50, 75:25	13
7	Toluene	0.50	—	1.5	2	110	66, 75:25	15
8	Toluene	0.25	—	3.0	2	110	51, 75:25	20
9	Toluene	0.10	—	1.5	48	T.A.	No reaction	
10	Toluene	0.10	BF_3-OEt_2	1.5	1	−78 °C–rt	Aromatization products	
11	CH_2Cl_2	0.10	BF_3-OEt_2	1.5	1	−78 °C–rt	Aromatization products	
1	Toluene	0.10	$Yb(OTf)_3$	1.5	1	−78 °C–rt	Aromatization products	

Yields were determined by NMR using 1,1,2-trichloroethylene as internal standard.
[a] Reaction run in sealed vial.

a quaternary center supporting the ester and one of the oxygen atoms of the diol moiety. For the oxo Diels–Alder reaction, harsher conditions with a higher temperature were required to ensure complete conversion of the reaction. Compound **14** was the only product isolated with very good yield (Scheme 6a). NMR analysis showed complete regio- and stereoselectivity for the process, obtaining only one diastereomer, *anti-endo*, which was identified by NOE analysis (Scheme 6b). This selectivity is remarkable since there is no evident polarization in the diene moiety that could account for the observed regioselectivity. In addition, previous reports of [4 + 2] cycloadditions under these systems have shown mixture of regioisomers when nitrosyl groups were used as dienophiles.[4c,4j,14]

Regarding the aza Diels–Alder reaction on substrate **4**, no expected isoquinuclidines were found, and only trace amounts of product **14** were isolated (probably because of decomposition of dienophile **5**). Again, *N*-tosylimine **5** showed less reactivity as a dienophile to these diene systems than ethyl glyoxylate.

Bicycles *endo*-**6** and *endo*-**7** were subjected to reductive ozonolysis conditions to afford the corresponding piperidine and tetrahydropyran (Scheme 7a) in good yields. *J*-coupling analysis[22] of compound **15** confirmed the stereochemical assignment (Scheme 7b), which is in agreement with the initially proposed structure of **6** (where the *anti*-correlation between the nitrogenated bridge and the isopropylidenedioxy group was proposed according to previous reports). It is noticeable that the ester present in **6** was conserved during the reductive conditions to **15**, while the same functionality in *endo*-**7** was reduced to a primary alcohol in **16** probably due to the presence of an alpha oxygen which facilitates the reduction process.[23]

In this manner, toluene can be converted into an enantiomerically pure polysubstituted piperidine or tetrahydropyrane containing five stereogenic centers in only four synthetic steps. This highlights the synthetic importance of the prepared bicyclo[2.2.2] octenes. *cis*-Cyclohexadienediols have been previously used to access polysubstituted heterocycles using different synthetic methodologies.[4b,18] The present study complements these previous reports on the use of enantiopure dienediols as starting materials for the preparation of the mentioned heterocycles.

2.2. Computational studies

In order to rationalize the regio- and stereoselectivity patterns for both types of Diels–Alder reactions using *cis*-cyclohexadienediols, we performed some theoretical calculations. High level ab initio methods have proved to give excellent results for energy barrier estimation of cycloaddition reactions.[24] Besides, these electronic structure calculations have been previously used to predict stereospecificities and to understand the mechanism of Diels–Alder reactions.[25] Therefore, we performed quantum chemical calculations on some of the cycloaddition reactions at the B3LYP/6-31+G (d,p) level of theory. This allowed us to thermodynamically and structurally characterize the transition states and related minima.

2.2.1. Diels–Alder reactions on diene 1a

The thermodynamic, kinetic and structural results are shown in Table 2. In agreement with the experimental data, the computational results suggest that in the oxo Diels–Alder reaction on **1a,** the most kinetically favored product is the *anti-endo* (Scheme 5a). This is also the preferred adduct from a thermodynamic point of

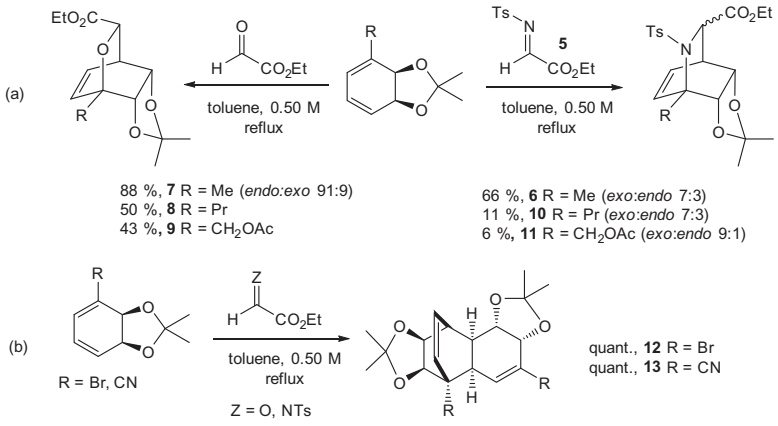

Scheme 5. Substrate scope for cycloadditions using ethyl glyoxylate and *N*-tosylimine **5** with *cis*-cyclohexadienediols obtained by biotransformation using *E. coli* JM109 (pDTG601).

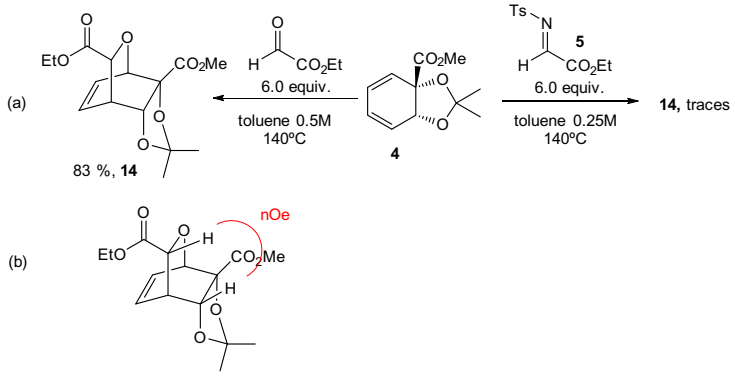

Scheme 6. Cycloadditions using ethyl glyoxylate and *N*-tosylimine **5** with *cis*-cyclohexadienediol **4** obtained by biotransformation using *Ralstonia eutropha* B9.

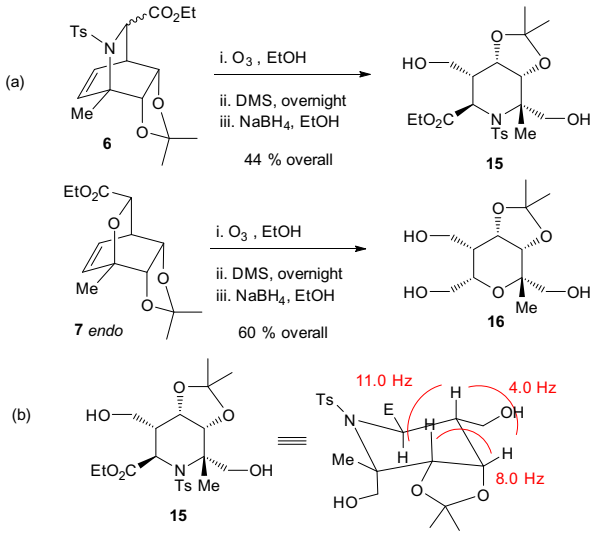

Scheme 7. Preparation of 2,2,3,4,5,6-hexasubstituted piperidine and tetrahydropyran.

view (see $\Delta G_{reaction}$ values), although this trend is not followed by all the systems, thus suggesting a kinetic control of the reactions. In fact, under this assumption, the calculated Curtin–Hammet product ratio is 93:6 *anti-endo*/*anti-exo*, which is close to the observed diastereomeric proportion. For the imino Diels–Alder reaction on **1a**, the theoretical data points to the formation of two kinetically favoured products, *anti-exo*/*anti-endo*, with an expected ratio of 62:38. This outcome is in agreement with the experimental diastereomeric mixture (7:3, Scheme 4a), showing the excellent performance of the computational model at predicting the stereoselectivity of these hetero Diels–Alder reactions. The activation energy for the aza Diels–Alder reaction is predicted to be higher than the oxo one, giving an explanation for the decrease in the yield from product **7** to **6** (Scheme 5a).

It is also noteworthy that the activation free energy ($\Delta G^{\ddagger}$) for the cycloadditions is significant (see Table 3). This is caused by a combination of a negative entropic factor and the use of high temperatures to allow the reactants to overcome the activation barrier, caused mainly by a substantial structural deformation at the transition state. The interaction between this geometrical distortion and the attractive and repulsive forces at the transition state seems to be quite different for the various cycloadditions, since the activation free energies span a range of 35–54 kcal/mol.

Figure 1 shows the optimized geometries and charge distribution of diene **1a** and both dienophiles. As expected by the bulky nature of the isopropylidene group, both Diels–Alder reactions on **1a** occur by the coupling of the dienophiles on the diene less hindered face, *anti* to the isopropylidene group. The electron-rich negatively charged zones (in red) are strongly localized over the oxygen atoms, while electron-poor positive zones (in blue) are largely restricted to the hydrogen atoms. This charge distribution points to significantly polar diene and dienophile molecules, whose interaction in an apolar solvent is electrostatically driven. Indeed, the *anti*-attack allows for a better fit between the negative and positive zones of the reactants, thus decreasing the electrostatic (and steric) repulsion.

It is worth analyzing the electronic features that affect the energy of the transition structures, and with that, the stereoselectivity. The perturbation theory,[26] provides a method to qualitatively estimate the slope of an early part of the path along the reaction coordinate leading up to the transition state (ΔE). The steeper path is likely to lead to the higher-energy transition structure. Two major factors influence the ΔE: the Coulombic repulsion or attraction between the reacting atoms and the HOMO–LUMO interaction of the reactants. The first factor is modulated by the atomic charges on the reacting atoms, whose values are shown in Figure 1. The experimentally observed connectivity allows for a complementary fit of the charges (Scheme 5a), in which the dienophile heteroatom is always linked to the diene quaternary carbon C3. The second term is controlled by the features of the frontier orbitals involved in the cycloaddition. For both hetero Diels–Alder reactions, the calculated HOMO/LUMO energy gap indicates a normal electronic demand ($HOMO_{diene} \rightarrow LUMO_{dienophile}$, Table 3), with both molecular orbitals being centered at the reacting atoms (Fig. 2). Given the above-mentioned connectivity, the symmetry of the frontier orbitals is in accordance with the observed *endo* preference when using ethyl glyoxylate as a dienophile, leading to an HOMO–LUMO constructive overlap. However, the *exo* spatial arrangement is slightly preferred in **6** (Table 2), thus revealing that there must be some special structural features at the transition state that explain this unexpected outcome (see below). Overall, the obtained stereoselectivity seems to be supported by a complex combination of electrostatic, electronic and structural factors.

2.2.2. Diels–Alder reactions on substrate 4

We performed the same computational analysis on the hetero Diels–Alder processes using diene **4**, and the results are summarized in Table 2. Again, the theoretical data are in close agreement with the experimental findings (Scheme 6a). Under kinetic control, the reaction between **4** and ethyl glyoxylate gives rise to a unique product *anti-endo* **14**, with an activation energy significantly lower than for the other possible Diels–Alder adducts. Conversely, when dienophile **5** is used, no imino Diels–Alder product is observed. The computational results show an increase of 10.9 kcal/mol in the

Table 2
ΔG values (under the experimental conditions), activation energy and products ratio for the Diels–Alder reactions

System		Product	$\Delta G_{reaction}$ (kcal/mol)	E_a (kcal/mol)	Product ratio[a]	Structural parameters[e]			Δd	$\Delta\omega$ (eV)
						$X_{O\cdots O}$ (Å)[b]	$X_{C-H\cdots O}$ (Å)[c]	X_p (Å)[d]		
Diene **1a**	Ethyl glyoxylate	*anti-endo* **7**	6.9	16.8	93	5.40	2.74 (3)	2.22 (1)	0.19	1.21
		anti-exo **7**	8.1	18.7	6	4.80	2.55 (3)	2.88 (2)	0.18	
		syn-endo	8.3	20.2	1	4.55	2.85 (3)	2.63 (2)	0.08	
		syn-exo	13.0	25.9	0	3.70	2.48 (3)	2.74 (2)	0.18	
	Dienophile **5**	*anti-exo* **6**	14.0	19.4	62	4.67 (2)	2.55 (3)	6.04 (3)	0.85	1.38
		anti-endo **6**	8.9	19.5	38	4.62 (3)	2.61 (5)	5.63 (2)	1.02	
		syn-endo	17.2	30.8	0	4.01 (5)	2.47 (5)	5.46 (3)	0.88	
		syn-exo	19.8	33.2	0	3.74 (4)	2.44 (3)	5.14 (3)	0.11	
Diene **4**	Ethyl glyoxylate	*anti-endo* **14**	9.6	18.6	97	5.2	2.77 (2)	2.42 (2)	0.11	1.00
		anti-exo	9.9	21.7	2	4.5	2.66 (3)	2.81 (2)	0.18	
		syn-endo	10.8	22.2	1	5.5	2.75 (3)	2.61 (2)	0.01	
		syn-exo	14.2	28.2	0	4.9	2.62 (4)	2.81 (3)	0.15	
	Dienophile **5**	*anti-endo*	10.4	29.5	75	3.24 (3)	2.52 (5)	6.71 (3)	1.11	1.17
		syn-exo	9.7	30.8	15	3.15 (2)	2.45 (3)	5.74 (3)	0.41	
		anti-exo	9.5	30.9	10	3.37 (2)	2.55 (3)	6.62 (3)	0.22	
		syn-endo	10.7	34.9	0	3.54 (3)	2.54 (5)	6.23 (3)	0.33	

The structural parameters and asynchronicity (Δd) of the transition states and the electrophilicity difference of the reactants ($\Delta\omega$) are also listed.
[a] According to the Curtin–Hammet principle.
[b] $X_{O\cdots O}$ denotes the average distance of disfavorable O···O interactions between both reactants moieties. For the systems containing the dienophile **5**, only the interactions below 5 Å were taken into account.
[c] $X_{C-H\cdots O}$ represents the average distance of favorable $C-H_{diene}\cdots O_{dienophile}$ interactions below 3 Å.
[d] X_p estimates the average distance of disfavorable interactions between the positively charged bulky groups of both reactants moieties. For the ethyl glyoxylate-containing systems, X_p represents the mean distance of H···H interactions (<3 Å). For the rest of the systems, X_p is calculated as the average C···C distance (<7 Å) between the $-CH_2-$ ester group and the sulfur-attached carbon atom of the tosyl group in **5**, and the methyl group from the ester moiety in diene **4**, the aromatic methyl group of diene **1a**, and the isopropylidene quaternary carbon atom of both dienes.
[e] The number of the interactions considered are shown between brackets.

Table 3
Activation free energy (under the experimental conditions) and HOMO–LUMO energy gap for the studied hetero Diels–Alder processes

System		Product	$\Delta G^{\ddagger}$ (kcal/mol)	HOMO–LUMO energy gap (kcal/mol)	
				Diene → dienophile	Dienophile → diene
Diene **1a**	Ethyl glyoxylate	*anti-endo* **7**	35.4	81.0	142.4
		anti-exo **7**	37.4		
		syn-endo	38.6		
		syn-exo	45.3		
	Dienophile **5**	*anti-exo* **6**	38.4	77.4	143.0
		anti-endo **6**	38.8		
		syn-endo	50.9		
		syn-exo	54.4		
Diene **4**	Ethyl glyoxylate	*anti-endo* **14**	38.7	89.1	136.6
		anti-exo	42.0		
		syn-endo	42.3		
		syn-exo	48.6		
	Dienophile **5**	*anti-endo*	50.9	85.6	137.3
		syn-exo	52.3		
		anti-exo	52.6		
		syn-endo	56.8		

activation energy barrier of this process, which in turns explains the need for drastic experimental conditions to ensure satisfactory conversions. This leads to a high $\Delta G^{\ddagger}$ value (50.9 kcal/mol, Table 3), which slows the reaction and allows the dienophile to first decompose in the system.

The optimized geometry and electrostatic potential of **4** are depicted in Figure 1. Given the size and charge distribution of the ester and isopropylidene groups, significant steric and electrostatic interactions with the dienophiles are expected. Therefore, the aza and oxo Diels–Alder attacks should proceed *anti* to the isopropylidene group, thus giving rise to the *anti-endo* adduct as the kinetically favoured product. The repulsion forces are so considerable in the presence of **5**, that the formation of the expected Diels–Alder bicycle is precluded.

The electronic features were also analyzed (Table 3), and a normal electronic demand was found. Again, the best fit of the positive and negative atomic charges of diene and dienophiles (Fig. 1) leads to the expected connectivity in each system. Remarkably, from **1a** to **4** the charges on the reacting carbon atoms vary to a great extent, causing the observed connectivity to invert (compare adducts **7** and **14**). This can be rationalized by taking into account the structural differences between both dienes. The presence of a deactivating ester group in **4** removes electron density from the π system, thus increasing the charge on C2. Additionally, the elimination of the aromatic methyl group from **1a** allows one of the isopropylidene oxygen atoms to approach and donate electron density to C5, negatively charging it. However, since there is no great difference in the atomic charges for C2 and C5 in **4**, we have performed the same computational analysis for the reversed connectivity; the results showed higher activation energy barriers (not shown). As expected, HOMO and LUMO orbitals are localized at the reacting atoms (Fig. 2) and, considering the observed

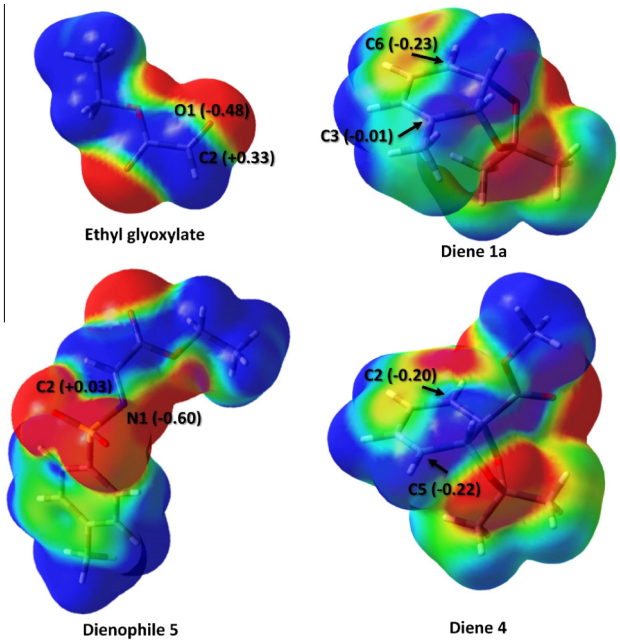

Figure 1. DFT optimized geometries for the dienes **1a** and **4**, and dienophiles ethyl glyoxylate and its *N*-tosyl imine **5**. In all cases, the electrostatic potential is mapped on an isodensity surface (isodensity value = 0.002 e, scale: -0.02 V (red) to 0.02 V (blue)). The labels for the reacting atoms are also shown with the NPA atomic charges between brackets. Color code: C (gray), H (white), O (red), N (blue), S (yellow).

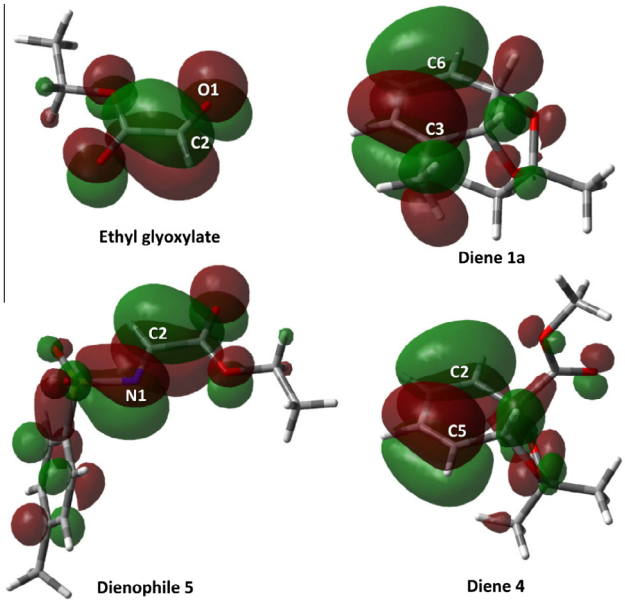

Figure 2. Spatial distribution of the HOMO for the dienes **1a** and **4**, and LUMO for the dienophiles ethyl glyoxylate and its *N*-tosyl imine **5**. The isodensity value is 0.0004 e. Color code: C (gray), H (white), O (red), N (blue), S (yellow).

connectivity, their constructive overlap supports the observed *endo* arrangement.

2.2.3. Structural determinants

The electrostatic and steric interactions seem to have a key impact in the yield and stereoselectivity. Both factors play a role in modulating the structure and energy of the transition states and products. To deeply understand how the different interactions exert those effects, it is worth analyzing the structural determinants behind the kinetic preference of the reactions. To aid the discussion, the thermodynamic and structural parameters of all the transition states can be found in Tables 2 and 3, while the optimized geometries and charge distribution for the most stable of them are depicted in Figure 3.

In general, the most stable transition states (TS) for the studied hetero Diels–Alder reactions (Fig. 3) are able to better separate the equally charged groups allowing to relieve the electrostatic and steric repulsion. This is evident when looking at their structural parameters (Table 2). For the systems containing diene **1a**, the average distance of disfavorable O···O interactions between the diene and dienophile moieties ($X_{O\cdots O}$) are larger for the lowest-energy transition states. Interestingly enough, the strength of the $C–H_{diene}\cdots O_{dienophile}$ hydrogen bonds is not a relevant structural determinant, since their average distance ($X_{C–H\cdots O}$) does not seem to correlate with the activation energy (E_a). When the dienophile **5** is present, it is also important to consider the repulsive interactions between the positively charged bulky groups, whose mean distance (X_p values) is higher for the observed TS. This is related to the unexpected stability of the *anti-exo* TS; while it is not favoured from an electronic point of view (destructive HOMO–LUMO overlap), this arrangement greatly relieves the electrostatic repulsion of the tosyl and isopropylidene groups, making it slightly more stable than the expected *anti-endo* TS (see Fig. 3 and Table 2). Likewise, a similar phenomenon occurs when **4** and **5** react, where an *endo*/*exo* product mixture is also predicted (though it is not experimentally evidenced because of the high-energy activation barrier). Therefore, it can be concluded that the use of the highly hindered dienophile **5** gives rise to a decrease in the *endo*/*exo* diastereoselectivity.

The same analysis for the cycloaddition on diene **4** is not straightforward. Even though the same structural parameters arise as relevant, the trends are not well defined. The preferred TS are those that minimize the electrostatic repulsion (high $X_{O\cdots O}$ and X_p values), relieving at the same time the steric hindrance through an *anti*-facial attack.

In order to characterize the polarity of the Diels–Alder reactions, the global electrophilicity difference ($\Delta\omega$) and the asynchronicity (Δd) were determined (Table 2). All the reactions involve an asynchronous bond formation, although this phenomenon is much more important when dienophile **5** is used, with Δd values that suggest a two-step mechanism.[27] Firstly, a C–C bond is formed through a nucleophilic/electrophilic two-center interaction. After that, the formation of the C–N bond begins, thus initiating the second stage of the reaction. Although there is not a strict linear relationship, an increase in the reaction polarity seems to be accompanied by an increase in its asynchronicity, and less drastic experimental conditions are required.[27] Indeed, the calculated average Δd values correlate with the global electrophilicity difference ($\Delta\omega$) (see Table 2). For a given diene, the imino Diels–Alder reaction has a more polar character than the oxo cycloaddition, but no decrease in the activation barrier was observed experimentally (Table 2). This fact stresses the relevance of the electrostatic and steric hindrance experienced by the TS when the ester and tosyl bulky groups are present in the dienophile, which counteracts the expected trend. Given a dienophile, diene **4** leads to a reduction in the reaction polarity, thus accounting for the need of more drastic conditions to reach high yields (compare Schemes 5a and 6a).

3. Conclusion

Herein we have studied the aza and oxo Diels–Alder cycloadditions of isopropylidene protected *cis*-cyclohexadienediols using ethyl glyoxylate and its *N*-tosyl imine as dienophiles. The expected

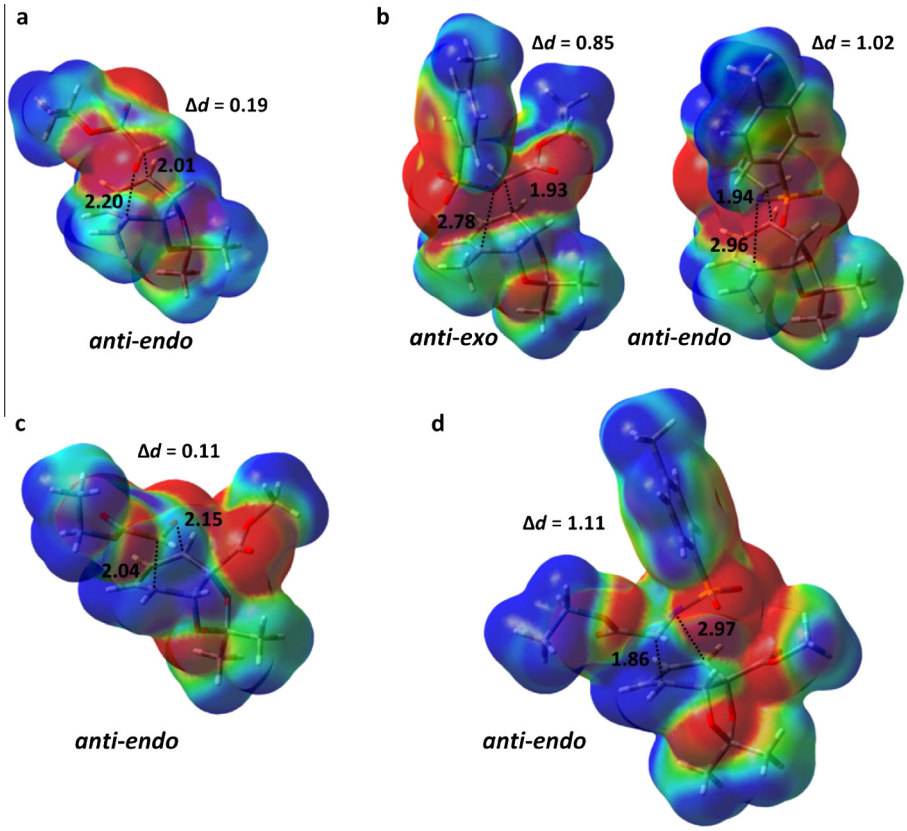

Figure 3. DFT optimized geometries for the most stable transition states corresponding to the Diels–Alder reactions between ethyl glyoxylate and **1a** (a), **5** and **1a** (b), ethyl glyoxylate and **4** (c), and **5** and **4** (d). The forming bonds are represented as dotted lines with their distances in Å. Asychronicity values (Δd) are also shown. In all cases, the electrostatic potential is mapped on an isodensity surface (isodensity value = 0.002 e, scale: -0.02 V (red) to 0.02 V (blue)). Color code: C (gray), H (white), O (red), N (blue), S (yellow).

heterocyclic bicyclo[2.2.2]octanes were obtained and fully characterized by spectroscopic methods. Excellent regio- and stereoselectivities were found for both types of cycloadditions. Quantum chemical calculations at the B3LYP/6-31+G(d,p) level of theory were performed to rationalize the observed selectivities. Excellent agreement of the used computational models with the experimental results was found, which allowed us to rationalize the experimental reactivity trends. In addition, as an example of the synthetic importance of the preparation of these bicyclo[2.2.2]octanes, the enantiopure preparation of a 2,2,3,4,5,6-hexasubstituted piperidine and tetrahydropyran from toluene in only four synthetic steps has been described.

4. Experimental

4.1. General

All solvents were distilled prior to use. Mass spectra (MS) were recorded on a Shimadzu GC–MS QP 1100 EX instrument using the electron impact mode (70 eV). High resolution mass spectra were obtained on a Bruker Daltonics Q-TOF spectrometer (ESI mode), at Polo Tecnólogico de Pando, Facultad de Química, Universidad de la República. Infrared spectra (IR) were recorded either on neat samples (KBr disks) or in solution on a Shimadzu FT-IR 8101A spectrophotometer. NMR spectra were obtained in $CDCl_3$ on a Bruker Avance DPX-400 or a Bruker Avance III 500 instruments as indicated. Proton chemical shifts (δ) are reported in ppm downfield from TMS as an internal reference, and carbon chemical shifts are reported in ppm relative to the center line of the $CDCl_3$ triplet (77.0 ppm). Optical rotations were measured on a Zuzi 412 polarimeter using a 0.5 dm cell. $[\alpha]_D$ values are given in units of deg cm^2 g^{-1} and concentration values are expressed in g/100 mL. Analytical TLC was performed on silica gel 60F-254 plates and visualized with UV light (254 nm) and/or *p*-anisaldehyde in acidic ethanolic solution. Flash column chromatography was performed using silica gel (Kieselgel 60, EM reagent, 230–400 mesh) Chemicals and reagents were purchased from Sigma–Aldrich and used as received. *E. coli* JM109 (pDTG601) was generously donated by Prof. David T. Gibson (1938–2014). All of his strain collections are currently managed by Prof. Rebecca Parales (University of California, Davis). *Ralstonia eutropha* B9 was generously donated by Prof. Andrew G. Myers (Harvard University-USA). Shake-flask cultivation was carried out using a Thermo Forma orbital shaker. A Sartorious-Biostat A plus bioreactor fitted with a 5 liter baffled vessel was used as bioreactor.

4.2. Biotransformation procedures

4.2.1. Media composition

Luria–Bertani (LB) medium used for cell growth contained: Bacto-Tryptone (10 g/L), Bacto-Yeast Extract (5 g/L), and sodium chloride (10 g/L). Agar (15 g/L) was added for solid media. When needed the medium was supplemented with sterile ampicillin sodium salt (0.1 g/L).

Mineral Salts Broth (MSB) used for the precultures for E. coli JM109 (pDTG601) contained: K_2HPO_4 (16 g/L), KH_2PO_4 (14 g/L), $(NH_4)_2SO_4$

(5 g/L), Bacto-Yeast Extract (15 g/L); after sterilization the medium was supplemented with sterile glucose (30 g/L), $MgSO_4{\cdot}7H_2O$ (2 g/L) and ampicillin sodium salt (0.1 g/L).

LB II used for cell growth and precultures of Ralstonia eutropha B9 contained: Tryptone (10 g/L), Yeast Extract (5 g/L), $CaCl_2{\cdot}2H_2O$ (1 g/L), $MgCl_2$ (0.05 g/L). Agar (15 g/L) was added for solid media.

Bioreactor defined mineral salt medium for E. coli JM109 (pDTG601) consisted of: KH_2PO_4 (7.5 g/L), citric acid (2.0 g/L), $MgSO_4{\cdot}7H2O$ (5.0 g/L), ferric ammonium citrate (0.3 g/L), 98% H_2SO_4 (1.4 mL/L) and trace metal solution (1.5 mL/L). After sterilization, pH is regulated to 6.8 by the addition of conc. ammonium hydroxide, followed by supplementation with sterile thyamine hydrochloride (0.3 g/L) and ampicillin sodium salt (0.1 g/L). Trace metal solution contained: citric acid (40 g/L), $MnSO_4{\cdot}2H_2O$ (30 g/L), NaCl (10 g/L), $FeSO_4{\cdot}7H_2O$ (1 g/L), $CoCl_2{\cdot}6H_2O$ (1 g/L), $ZnSO_4{\cdot}7H_2O$ (1 g/L), $CuSO_4{\cdot}5H_2O$ (0.1 g/L), H_3BO_3 (0.1 g/L), $NaMoO_4{\cdot}2H_2O$ (0.1 g/L); pH was adjusted to 3.0 with ammonium hydroxide.

Bioreactor defined mineral salt medium for Ralstonia eutropha B9 consisted of: KOH (0.4 g/L), Nitriloacetic acid (0.2 g/L), $MgSO_4$ (0.28 g/L), $CaCl_2{\cdot}2H_2O$ (0.07 g/L), $(NH_4)Mo_2O_{24}{\cdot}6H_2O$ (0.2 mg/L), $FeSO_4$ (2 mg/L), Hutner's Metal Solution* (1 mL/L), NH_4SO_4 (1 g/L), KH_2PO_4 (2.72 g/L), Na_2HPO_4 (2.84 g/L).

*Hutner's Metal Solution composition:[28] EDTA (5 g/L), $ZnSO_4{\cdot}7H_2O$ 22 g/L, $FeSO_4{\cdot}7H_2O$ (10 g/L), $CuSO_4$ (3.9 g/L), $CoNO_3{\cdot}6H_2O$ (0.5 g/L), $NaBO_4{\cdot}10H_2O$ (0.36 g/L), H_2SO_4 (1 mL/L), H_2O up to 1L.

4.2.2. Plate preparation

E. coli JM109 (pDTG601) cells properly stored in cryovials, are streaked into LB-agar plates (supplemented with ampicillin sodium salt). The streaked plate is incubated at 37 °C for 24 h. Single-cell colonies are chosen for the precultures preparation. *Ralstonia eutropha* B9 cells properly stored in cryovials are streaked into LBII-agar plates and incubated at 30° C over 48 h. Single-cell colonies are chosen for the precultures preparation.

4.2.3. Biotransformations in bioreactors

Bioreactor cultures and biotransformations using E. coli JM109 (pDTG601). Growth and biotransformation in the bioreactor using *E.coli* JM109 (pDTG601) were carried out using a modification of our previously published procedure.[3b] Thus, 5 mL of LB medium supplemented with ampicillin sodium salt (0.1 g/L) and glucose (5 g/L) were inoculated with a single colony of *E. coli* JM109 (pDTG601), and grown overnight at 37 °C and 150 rpm. Two 500 mL shake-flasks containing 150 mL of MSB medium were inoculated with 1 mL of the grown culture. These preculture flasks were placed in an orbital shaker at 37 °C and 150 rpm, for 12 hrs. Both entire cultures were used to inoculate the bioreactor (Sartorius Biostat A plus), charged with an initial volume of 2.5 L, and set to 500 rpm, 30 °C, and air flow rate of 4L/min. The pH value was controlled automatically to 6.8 by addition of conc. ammonium hydroxide during the whole process. A pulse of antifoam agents (Aldrich's Antifoam Y: Silicone dispersion in water 1:1) was added at the beginning of the run. At 6 h after inoculation the dissolved oxygen value sharply increased (indicating carbon deprivation), whereupon a glucose fed-batch was started by adding glucose (0.7 g/mL solution) from an initial rate of 0.08 mL/min to 0.54 mL/min in a 20 h period. When the biomass concentration reached 15 g/L cdw, IPTG was added to induce toluene dioxygenase expression (IPTG final concentration in bioreactor of 10 mg/L), and the stirrer speed was set to 900 rpm. After the culture reached the stationary phase (c.a. 26 h, 50 g/L cdw aprox), glucose feeding was decreased to 0.25 mL/min and substrate addition was started. A solution of the corresponding substrate in liquid paraffin (0.5 M) was added at a flow rate of 20 mL/min using a peristaltic pump. After the biotransformation was completed, the pH of the medium in the bioreactor was adjusted to 7.5. The culture broth was centrifuged at 7000 rpm and 4 °C for 30 min, the supernatant was collected and the cell pellet properly disposed. Centrifugation led to the separation of the liquid paraffin (which contains no detectable amounts products) from the aqueous phase. The latter was properly lyophilized overnight to obtain a dry powder, which was extracted several times with ethyl acetate until no more diols were detected by TLC. The solvent was evaporated to afford the corresponding diol, which was washed several times with hexanes to remove the liquid paraffin traces.

Bioreactor cultures and biotransformations using Ralstonia eutropha B9. Two 500 mL flasks containing 90 mL of LBII medium were inoculated with a single colony of *Ralstonia eutropha* B9 and grown over 48 h at 28 °C, 150 rpm. Both entire cultures were used to inoculate the bioreactor (Sartorius Biostat A plus), charged with an initial volume of 3 L, and set to 300 rpm, 30 °C, and air flow rate of 3 L/min. An initial volume of 17.5 mL of 1.5 M fructose solution was added. The pH value was controlled automatically at 7.4 by the addition of concentrated ammonium hydroxide during the whole process. After 20 h a second pulse of 1.5 M fructose solution (19 mL) was added along with a first pulse of 1.5 M sodium benzoate solution (4.3 mL). From this time on, 8 mL of both solutions (fructose and sodium benzoate) were added every 4 h over 3.5 days using a peristaltic pump. Stirring was adjusted when needed, (based on the oxygen profile of the process) reaching at the end 600 rpm. After this, the culture broth was centrifuged at 7000 rpm and 4 °C for 30 min, the supernatant was collected and the cell pellets were properly disposed. The resulting media (which contained 27 g/L of **2**) was lyophilized to obtain a white solid, which had a 79% content on diol **2** (determined by NMR using sodium acetate as internal standard). This solid is stable and can be stored at room temperature in a proper dessicator.

4.3. Synthetic protocols and compounds characterization

4.3.1. (1*S*,6*R*)-Methyl 1,6-isopropylidenedioxycyclohexa-2,4-dienecarboxylate 4[4h]

The lyophilized culture medium was cooled to 0 °C, suspended on dimethoxypropane and 6 equiv of TFA were added. The reaction mixture was stirred at room temperature for 24 h after which it was filtered through a pad of Celite. After solvent evaporation in vacuo, a solution of diazomethane in diethylether (3 equiv) was added dropwise. The product was purified by column chromatography using SiO_2 as the stationary phase. Diazomethane ether solution was prepared by the decomposition of *N*-nitroso-*N*-methylurea using a bi-phasic system oh KOH 10% and diethyl ether. ^{1}H NMR (400 MHz, $CDCl_3$) δ 6.18–6.09 (m, 2H), 6.08–6.01 (m, 1H), 5.88–5.80 (m, 1H), 4.98 (dd, J = 4.3, 0.7 Hz, 1H), 3.81 (s, 3H), 1.46 (s, 3H), 1.44 (s, 3H); ^{13}C NMR (100 MHz, $CDCl_3$) δ 172.2, 124.7, 124.5, 124.1, 124.0, 106.8, 79.4, 72.7, 53.0, 26.9, 25.2.

4.3.2. General procedure for the oxo Diels–Alder reaction

To a 0.5 M solution of the corresponding diene in dry toluene under an N_2 atmosphere, ethyl glyoxylate (1.5 equiv, except for diene **4** where 8 equiv were used) was added and the reaction mixture heated at reflux until consumption of the starting material. The reaction was monitored by thin layer chromatography. After the starting material had disappeared, the toluene was evaporated in vacuo. The product was purified by column chromatography using SiO_2 as stationary phase.

4.3.2.1. (1*S*,3*S*,4*R*,7*S*,8*S*)-Ethyl 7,8-isopropylidenedioxy-1-methyl-2-oxabicycle[2.2.2]-5-octen-3-carboxylate *endo*-7. ^{1}H NMR (500 MHz, $CDCl_3$) δ (ppm) = 6.18–6.10 (m, 2H), 4.42 (ddd, J = 7.1, 3.6, 1.0 Hz, 1H), 4.21–4.14 (m, 3H), 4.07 (dd, J = 7.1, 0.9 Hz, 1H), 3.48 (ddt, J = 7.6, 3.7, 1.9 Hz, 1H), 1.58 (s, 3H), 1.32 (s, 3H), 1.31

(s, 3H), 1.26 (t, J = 7.1 Hz, 3H); ^{13}C NMR (125 MHz, $CDCl_3$) δ 171.3, 135.8, 128.3, 109.6, 80.6, 75.5, 73.1, 70.5, 61.1, 39.0, 25.6, 25.3, 21.3, 14.2; IR (cm^{-1}) = 2980, 2936, 2899, 1759, 1726, 1205, 1173, 1063; MS (EI, 70 eV) m/z (rel. int.): 73.05 (100), 81.10 (44), 97.10 (70), 256.20 (20); HRMS (ESI^+) calcd for $C_{14}H_{20}O_5$ = 291.1203 (M +Na^+) found 291.1277; $[\alpha]_D^{21}$ = −51 (c 0.9, MeOH).

4.3.2.2. (1*S*,3*S*,4*R*,7*R*,8*S*)-Ethyl 7,8-isopropylidenedioxy-1-methyl-2-oxabicycle[2.2.2]-5-octen-3-carboxylate *exo*-7. ^{1}H NMR (500 MHz, $CDCl_3$) δ (ppm) = 6.34 (ddd, J = 8.0, 6.7, 0.9 Hz, 1H), 6.10 (ddd, J = 8.0, 1.1, 1.1 Hz, 1H), 4.30–4.16 (m, 4H), 3.86 (d, J = 2.0 Hz, 1H), 3.37–3.33 (ddt, J = 7.0, 3.6, 1.7 Hz 1H), 1.56 (s, 3H), 1.32–1.23 (m, 9H); ^{13}C NMR (125 MHz, $CDCl_3$) δ 171.3, 134.9, 131.0, 109.0, 80.2, 73.7, 72.8, 71.8, 61.3, 38.3, 25.6, 25.2, 21.2, 14.2.

4.3.2.3. (1*S*,3*S*,4*R*,7*S*,8*S*)-Ethyl 7,8-isopropylidenedioxy-1-propil-2-oxabicycle[2.2.2]-5-octen-3-carboxylate 8. ^{1}H NMR (400 MHz, $CDCl_3$) δ (ppm) = 6.19 (d, J = 8.4 Hz, 1H), 6.11 (dd, J = 8.4, 6.3 Hz, 1H), 4.39 (dd, J = 7.1, 3.5, 1.0 Hz, 1H), 4.17–4.06 (m, 3H), 3.43 (ddd, J = 7.3, 3.5, 1.7 Hz, 1H), 1.33 (s, 3H), 1.95 (ddd, J = 14.2, 11.8, 4,9 Hz, 3H), 1.71 (d, J = 4.6 Hz, 1H), 1.73–1.66 (m, 1H), 1.66–1.59 (m, 1H), 1.57–1.49 (m, 1H), 1.28 (s, 3H), 1.27 (s, 3H), 1.23 (t, J = 7.1 Hz, 3H) 0.98 (t, J = 7.2 Hz, 3H); ^{13}C NMR (100 MHz, $CDCl_3$) δ (ppm) = 171.4, 134.3, 128.5, 109.5, 79.7, 75.6, 75.4, 70.3, 60.9, 38.9, 36.9, 25.6, 25.2, 16.5, 14.5, 14.1; IR (cm^{-1}): 2978, 2961, 2936, 2911, 2876, 1759, 1728, 1373, 1207, 1165, 1072, 1030; MS (EI, 70 eV) m/z (%): 91.10 (44), 123.15 (100), 165.10 (84), 295 (M+, 16); $[\alpha]_D^{21}$ = −7.4 (c 1.1, MeCN).

4.3.2.4. (1S,3S,4R,7S,8S)-Ethyl-7,8-isopropylidenedioxy-1-(acetoxymethyl)-2-oxabicyclo[2.2.2]-5-octen-3-carboxylate 9. ^{1}H NMR (400 MHz, $CDCl_3$) δ (ppm) = 6.16 (d, J = 1.4 Hz, 1H), 6.15 (dd, J = 1.8, 1.1 Hz, 1H), 4.52 (dd, J = 12.2, 1.5 Hz, 1H), 4.42 (ddd, J = 7.1, 3.0, 1.0 Hz, 1H), 4.31 (dd, J = 12.2, 1.4 Hz, 1H), 4.27 (dd, J = 7.1, 1.1 Hz, 1H), 4.17 (t, J = 1.6 Hz, 1H), 4.11 (ddd, J = 7.1, 6.5, 1.6 Hz, 1H), 3.47 (dtd, J = 6.4, 3.4, 1.7 Hz, 1H), 2.10–2.09 (m, 3H), 2.08–1.99 (m, 1H), 1.25 (t, J = 1.5 Hz, 6H), 1.20 (td, J = 7.1, 1.6 Hz, 3H); ^{13}C NMR (100 MHz, $CDCl_3$) δ (ppm) = 170.8, 170.7, 131.4, 129.2, 110.1, 75.9, 75.0, 74.2, 70.0, 64.6, 61.1, 39.6, 25.5, 25.2, 20.8, 14.1; IR (cm^{-1}): 2984, 2937, 1748, 1242, 1209, 1057; MS (EI, 70 eV) m/z (rel. int.): 107.1 (70), 153.1 (100), 195.1 (72), 208.1 (51), 212.1 (M+, 51); HRMS (ESI^+) calcd for $C_{14}H_{20}O_5$-Na = 349.1258 (M+Na^+) found 349.1334; $[\alpha]_D^{21}$ = −23.6 (c 1.2, MeOH).

4.3.2.5. (1*S*,3*S*,4*S*,7*R*,8*S*)-3-Ethyl -8-methyl-7,8-isopropylidenedioxy-2-oxabicycle[2.2.2]5-octene-3,8-dicarboxylate 14. ^{1}H NMR (400 MHz, $CDCl_3$) δ (ppm) = 6.46 (ddd, J = 7.3, 5.6, 1.5 Hz, 1H), 6.25 (t, J = 7.3 Hz, 1H), 5.02 (d, J = 3.8 Hz, 1H), 4.89 (dd, J = 5.3, 1.3 Hz, 1H), 4.23 (d, J = 1.6 Hz, 1H), 4.18 (dq, J = 7.3, 1.3 Hz, 2H), 3.85 (s, 3H), 3.62 (dddd, J = 6.4, 4.0, 1.7, 1.7 Hz, 1H), 1.33 (s, 3H), 1.27 (s, 3H), 1.26 (t, J = 7.2 Hz, 3H); ^{13}C NMR (100 MHz, $CDCl_3$) δ (ppm) = 172.1, 170.6, 131.1, 129.8, 111.4, 84.4, 77.4, 77.0, 76.7, 76.1, 69.6, 68.4, 61.4, 53.0, 38.8, 25.9, 25.7, 14.2.; IR (cm^{-1}): 2988, 2955, 2940, 1759, 1738, 1375, 1267, 1228, 1211, 1179, 1163, 1113, 1065, 1045, 1026, 897, 872, 856, 725; MS (EI, 70 eV) m/z (%): 60.05 (73), 73.05 (100), 83.15 (66), 97, 10 (55), 129.15 (54), 213,20 (14); HRMS (ESI^+) calcd for $C_{15}H_{20}O_7$ = 335,1090 (M +) found 335.1101; $[\alpha]_D^{21}$ = +162 (c 0.5, MeOH).

4.3.3. General procedure for the aza Diels–Alder reaction

The ethyl glyoxylate *N*-tosyl imine **5** was prepared using the procedure described by Le Goffic et al.[29] Ethyl glyoxylate was dissolved in dry toluene; followed by *p*-toluenesulphonyl isocyanate (1 equiv) and catalytic amounts of $AlCl_3$ (0.5% m/m of *p*-toluenesulphonylisocyanate) (final *p*-toluenesulphonylisocyanate concentration = 2 M). The mixture was heated at reflux for 4.5 h, after which it was cooled to 50 °C and used without any purification to the cycloaddition reaction. A 0.5 M solution of the corresponding diene in dry toluene was added to the freshly prepared *N*-tosyl imine. The mixture was heated at reflux until the starting material was consumed. The system was allowed to reach room temperature. Toluene was removed in vacuo and product was purified by chromatographic column using SiO_2 as the stationary phase.

4.3.3.1. (1*S*,4*S*,7*R*,8*S*)-Ethyl 7,8-isopropylidendioxy-1-methyl-2-tosyl-2-azabicycle[2.2.2]5-octenen-3-carboxylate *exo* and *endo*-6. *exo*-Isomer: ^{1}H NMR (400 MHz, $CDCl_3$): δ(ppm) = 7.96 (dt, J = 1.9, 8.3 Hz, 2H), 7.30 (d, J = 8.2 Hz, 2H); 6.22 ddd, J = 0.9, 6.7, 8.0 Hz, 1H), 5.96 (dt, J = 1.1, 8.1 Hz, 1H), 4.36 (ddd, J = 0.7, 3.5, 7.1 Hz, 1H), 4.31 (q, J = 7.2 Hz, 2H), 4.24 (d, J = 3.3 Hz, 1H), 4.16 (dd, J = 0.9, 7.1 Hz, 1H), 3.40 (dddd, J = 1.2, 3.4, 3.4, 6.7 Hz, 1H), 2.42 (s, 3H), 1.44 (s, 3H), 1.35 (t, J = 7.2 Hz, 3H), 1.25 (s, 3H), 1,23 (s, 3H); ^{13}C NMR (100 MHz, $CDCl_3$): δ(ppm) = 170.7, 135.7, 129.5, 128.0, 110.0, 81.0, 73.6, 61.7, 58.9, 58.7, 37.6, 25.5, 25.3, 21.6, 19.2, 14.2; *endo*-isomer: ^{1}H NMR (400 MHz, $CDCl_3$): δ(ppm) = 8.09 (dt, J = 1.9, 8.3 Hz, 2H), 7.30–7.28 (m, 2H); 6.07 (ddd, J = 0.9, 6.4, 7.6 Hz, 1H), 5.91 (ddd, J = 1.0, 1.6, 8.0 Hz, 1H), 4.60 (d, J = 2.4 Hz, 1H), 4.58 (dd, J = 1.0, 7.1 Hz, 1H), 4.53 (ddd, J = 1.0, 3.3, 7.1 Hz, 1H), 4.25–4.23 (dd, J = 0.9, 7.1 Hz, 1H), 3.52–4.48 (m, 1H), 2.42 (s, 3H), 1.39 (s, 3H) 1.32–1.27 (m, 9H); ^{13}C NMR (100 MHz, $CDCl_3$): δ(ppm) = 170.72, 143.49, 140.28, 136.43, 129.56, 129.46, 128.13, 109.64, 79.07, 76.04, 61.48, 58.78, 56.27, 39.75, 29.69, 26.90, 25.48, 22.66, 19.23; IR (/cm): 2986, 2937, 1746, 1375, 1118, 712; MS: m/z (Int. Rel) = 65.1 (22); 91.1 (98); 155.1 (58); 248.1 (100); 406.1 (6); HRMS (ESI^+) calcd for $C_{21}H_{27}NO_6$-SNa = 444.1457 (M+Na+) found 444.1451.

4.3.3.2. (1*S*,4*S*,7*R*,8*S*)-Ethyl 7,8-isopropylidendioxy-1-propyl-2-tosyl-2-azabicyclo[2.2.2]5-octene-3-carboxylate 10 *exo*- and *endo*-10. *exo*-isomer: ^{1}H NMR (400 MHz, $CDCl_3$) δ (ppm) = 7.84 (ddd, J = 8.4, 2.1, 1.8 Hz, 2H), 7.33–7.29 (m, 2H), 6.04 (ddd, J = 1.2, 7.0, 7.9 Hz, 1H), 5.82 (dt, J = 1.0, 8.0 Hz, 1H), 4.43 (dd, J = 7.0, 1.0 Hz, 1H), 4.34–4.28 (m, 3H), 4.17 (d, J = 3.5 Hz, 2H), 3.37 (dddd, J = 6.9, 3.5, 3.5, 1.2 Hz, 1H), 2.44 (s, 3H), 2.23–2.14 (m, 1H), 2.03–1.91 (m, 1H), 1.50–1.40 (m, 2H), 1.27 (s, 3H), 1.26 (t, J = 7.2 Hz, 3H);^{13}C NMR (100 MHz, $CDCl_3$) δ (ppm) = 172.1, 170.6, 131.1, 129.8, 111.4, 84.4, 77.4, 77.0, 76.7, 76.1, 69.6, 68.4, 61.4, 53.0, 38.8, 25.9, 25.7, 14.2.; *endo*-isomer: ^{1}H NMR (400 MHz, $CDCl_3$) δ (ppm) = 8.02 (ddd, J = 8.4, 2.1, 1.9 Hz, 2H), 7.34–7.29 (m, 2H), 6.12 (s, 1H), 6.11 (s, 1H), 4.65 (d, J = 2.9 Hz, 1H), 4.62 (d, J = 6.8 Hz, 1H), 4.42 (d, J = 7.0, 3.3 Hz, 1H), 4.16–4.11 (m, 2H), 3.50 (m, 1H), 2.44 (s, 3H), 2.23–2.14 (m, 1H), 2.03–1.91 (m, 1H), 1.50–1.40 (m, 2H), 1.27 (s, 3H), 1.26 (t, J = 7.2 Hz, 3H), 1.26–1.24 (m, 3H), 0.67 (t, J = 7.2 Hz, 3H); ^{13}C NMR (100 MHz, $CDCl_3$) δ (ppm) = 170.6, 133.9, 129.4, 129.3, 128.3, 109.4, 79.1, 75.9, 63.9, 61.7, 57.0, 39.4, 34.6, 34.2, 26.9, 25.0, 21.6, 14.3, 14.1;IR (cm^{-1}): 2974, 2937, 1751, 1373, 1352, 1325, 1209, 1180, 1163, 1078, 970, 710, 590, 550; MS (EI, 70 eV) m/z (rel. int.): 91.1 (79), 155.1 (85), 108.1 (35), 236.1 (34), 276.1 (97), 294.2 (37), 318.1 (100); HRMS (ESI^+) calcd for $C_{23}H_{21}NO_6SNa$ = 472.1764 (M+Na^+) found 472.1764.

4.3.3.3. (1*R*,4*S*,7*R*,8*S*)-Ethyl 1-(acetoxymethyl)-7,8-iopropylidenedioxy-2-tosyl-2-azabicycle[2.2.2]5-octen-3-carboxylate 11. ^{1}H NMR (400 MHz, $CDCl_3$): δ (ppm) = 7.93 (d, J = 8.3 Hz, 2H), 7.27–7.31 (m, 2H), 6.26 (ddd, J = 0.9, 6.7, 8.0 Hz, 1H), 5.95 (dt, J = 1.0, 8.0 Hz; 1H), 4.95 (d, J = 13.0 Hz; 1H), 4.60 (dd, J = 1.0, 7.1 Hz, 2H), 4.28–4.38 (m, 4H), 4.26 (d, J = 12.9 Hz, 1H), 3.49 (dddd, J = 1.2, 3.4, 3.4, 7.0 Hz, 1H), 2.42 (s, 3H), 1.64 (s, 3H), 1.36 (t, J = 7.1 Hz; 3H), 1.23 (s, 6H); ^{13}C NMR (100 MHz, $CDCl_3$): 170.3; 170.2;

143.7; 137.8; 131.7; 130.1; 129.4; 128.4; 110.4; 77.4; 77.1; 76.8; 76.2; 73.2; 61.5; 60.8; 58.4; 37.6; 25.5; 25.4; 21.5; 20.1; 14.2; IR (cm^{-1}): 2984, 2938, 1748, 1358, 1381, 1370, 1327, 1242, 1211, 1190, 1163, 1079, 1067, 966, 914, 882, 868, 733, 714, 669, 650, 588, 552; MS (EI, 70 eV) *m/z* (int. rel.): 91.1 (95), 155.1 (50), 196.1 (80), 224.1 (28), 306.1 (100), 324.2 (69); HRMS (ESI^+) calcd for $C_{23}H_{29}NO_8SNa$ = 502.1512, ($M+Na^+$) found 502.1506.

4.3.4. General procedure for the reductive ozonolysis

In a round-bottomed flask under N_2, the corresponding bicycle was dissolved in dry CH_2Cl_2 (up to a 0.07 M concentration). After the addition of pyridine (3 equiv), the solution was cooled to −78 °C and O_3 was bubbled until the disappearance of the starting material. The reaction mixture was then allowed to reach room temperature, diluted with CH_2Cl_2 and a saturated solution of $NaHCO_3$ was added. The aqueous phase was extracted three times with CH_2Cl_2. The combined organic phases were dried over Na_2SO_4 and the solvent was removed under reduced pressure.

4.3.5. General procedure for the reduction with $NaBH_4$

To a 0.1 M solution of the starting material in absolute ethanol at 0 °C, 4 equiv of $NaBH_4$ were added. The reaction mixture was stirred at room temperature overnight, after which an NH_4Cl saturated solution was added. After stirring for 10 min, the product was extracted 4 times with a 1:1 mixture of AcOEt/isopropanol. Purification was carried out by column chromatography using SiO_2 as the stationary phase.

4.3.5.1. (2*R*,3*R*,4*S*,5*R*,6*S*)-Ethyl 4,5-dihydroxy-3,6-bis(hydroxymethyl)-6-methyl-1-tosylpiperidine-2-carboxylate 15. ^1H NMR (400 MHz, $CDCl_3$) δ 7.81 (d, J = 8.3 Hz, 1H), 7.31–7.27 (m, 1H), 4.56 (dd, J = 8.2, 3.9 Hz, 1H), 4.50 (d, J = 11.1 Hz, 1H), 4.31–4.22 (m, 3H), 4.05 (d, J = 8.2 Hz, 1H), 3.98 (dt, J = 11.7, 3.8 Hz, 1H), 3.88 (ddd, J = 11.7, 8.8, 5.9 Hz, 1H), 3.73 (dd, J = 12.4, 9.3 Hz, 1H), 3.10 (dd, J = 9.4, 5.5 Hz, 0H), 2.53–2.43 (m, 1H), 2.41 (s, 1H), 1.60 (s, 1H), 1.34 (t, J = 7.1 Hz, 1H), 1.22 (s, 1H), 0.92 (s, 1H); ^{13}C NMR (100 MHz, $CDCl_3$) δ 173.2, 143.5, 139.4, 129.6, 127.6, 108.2, 78.8, 71.7, 66.7, 63.6, 62.2, 61.7, 56.7, 38.3, 24.8, 23.8, 23.3, 21.5, 14.0; IR (cm-1): 3476, 2884, 2940, 1738, 1329, 1260, 1159, 1088, 1040, 995, 880, 816, 548; MS (EI, 70 eV) *m/z* (int. rel.): 91.1 (100), 124.1 (73), 154.1 (56), 155.1 (53), 278.1 (93), 368.1 (28), 384.2 (57), 426.2 (75), 442.2 (15); HRMS (ESI^+) calcd for $C_{21}H_{31}NO_8SNa$ = 480.1668, ($M+Na^+$) found 480.1663; $[\alpha]_D^{21}$ = +17.1 (*c* 0.76, MeCN).

4.3.5.2. (2*S*,3*S*,4*S*,5*R*,6*S*)-2,5,6-Tris(hydroxymethyl)-3,4-isopopilidenedioxy-2-methyltetrahydro-2*H*-pyran-3,4-diol 16. ^1H NMR (400 MHz, $CDCl_3$) δ 4.59 (dd, J = 6.9, 5.1 Hz, 1H), 4.04 (d, J = 6.9 Hz, 1H), 3.91 (dt, J = 8.4, 4.2 Hz, 1H), 3.86 (d, J = 6.4 Hz, 2H), 3.73–3.68 (m, 2H), 3.67 (d, J = 1.0 Hz, 2H), 2.35 (p, J = 5.8 Hz, 1H), 1.55 (s, 3H), 1.36 (s, 3H), 1.34 (s, 3H); ^{13}C NMR (100 MHz, $CDCl_3$) δ (ppm) 109.0, 76.3, 72.8, 70.1, 68.4, 62.7, 60.0, 39.0, 25.8, 24.9, 20.9.; IR (cm^{-1}): 3347, 3327, 3292, 3269, 2980, 2933, 1377, 1265, 1209, 1161, 1065, 1049, 1020, 853; MS (EI, 70 eV) *m/z* (int. rel.): 73.1 (100), 81.1 (24), 97.1 (48), 111.1 (28), 129.2 (56), 247.2 (1), 256.2 (21); HRMS (ESI^+) calcd for $C_{12}H_{22}O_6Na$ = 285.1314, ($M+Na^+$) found 285.1309; $[\alpha]_D^{21}$ = −45.7 (*c* 0.8, MeOH).

4.4. Computational calculations

All geometry optimizations were performed in the gas phase and by means of the methods described hereinafter. Equilibrium geometries were characterized by the absence of imaginary frequencies, while all the first-order saddle-points were shown to have a Hessian matrix with a single negative eigenvalue, related to an imaginary vibrational frequency along the reaction coordinate. The animation of this negative normal mode was examined in each case, verifying that it reflects the change in geometry in going from reactants to products.

For the molecular modeling approach to the Diels–Alder cycloaddition reactions, different initial geometries of the reactants and products were built using the graphical model builder of Hyperchem,[30] and minimized interactively by means of the PM3 semiempirical method. Then, all the geometries were fully optimized employing the density functional theory method,[31] with the B3LYP hybrid functional[32] and the 6-31+G(d,p) basis set, as implemented in Gaussian 09.[33] This choice was supported by the wealth of computational literature on the Diels–Alder reactions, which points to this functional and similar basis sets to obtain consistent energetics.[34] The polarization function on hydrogen atoms was added for a better description of the hydrogen-mediated interactions involved in the Diels–Alder mechanism,[35] thus enhancing the reliability of the theoretical model in assessing the energetic and structural parameters that modulate the stereoselectivity. Starting from the optimized geometries of the products, the transition state structures were located by a series of standard first-order saddle-point optimizations, in which the forming C–C, C–O, and C–N bonds were initially fixed at various lengths.

The natural population analysis (NPA) phase of the natural bond orbital analysis (NBO) was used to estimate the atomic charges.[36] Zero-point energies and thermal corrections were taken from unscaled analytical vibrational frequencies. The products ratio under kinetic control was calculated according to the Curtin–Hammet principle.[37] The polarity of the Diels–Alder reactions were assessed through asynchronicity (Δd) and global electrophilicity (ω) parameters.[38]

Acknowledgments

The authors would like to thank the Agencia Nacional de Investigación e Innovacion (Project FCE 6045) for financial support and for a Ph.D. scholarship for Mariana Pazos. We would also like to thank the Comisión Sectorial de Investigación Científica—Universidad de la República for a MSc scholarship for María Agustina Vila. We thank Prof. Alejandra Rodríguez (Facultad de Química, Polo Tecnológico de Pando - UdelaR) for the High Resolution Mass Spectroscopy analysis and Prof. Guillermo Moyna and Gualberto Bottini (Departamento de Química del Litoral, CENUR Litoral Norte—UdelaR) for the NOE experiments and helpful discussions regarding the stereochemistry of the Diels–Alder cycloadducts. We also would like to thank Lucía Almeida and Gonzalo Macias for the NMR spectra of product *exo*-**7**.

References

1. (a) Banwell, M. G.; Gao, N.; Ma, X.; Petit, L.; White, L. V. *Pure Appl. Chem.* **2012**, *84*, 1329–1339; (b) Banwell, M. G.; Lehmann, A. L.; Rajeev, S. M.; Willis, A. C. *Pure Appl. Chem.* **2011**, *83*, 411–423; (c) Hudlicky, T.; Reed, J. W. *Synlett* **2009**, 0685–0703; (d) Johnson, R. A. In *Microbial Arene Oxidations*; John Wiley and Sons, Inc., 2004; Vol. 63,; (e) Banwell, M G.; Edwards, A. J.; Harfoot, G. J.; Jollife, K. A.; McLeod, M. D.; McRae, K. J.; Stewart, S. G.; Vogtle, M. *Pure Appl. Chem.* **2003**, *75*, 223–229; (f) Gonzalez, D.; Gibson, D. T.; Hudlicky, T. *Aldrichim. Acta* **1999**, *32*, 35–62; (g) Lewis, S. E. *Chem. Commun.* **2014**, 2821–2830.
2. (a) Feng, Y.; Ke, C. Y.; Xue, G.; Que, L. *Chem. Commun.* **2009**, 50–52; (b) Motherwell, W. B.; Williams, A. S. *Angew. Chem., Int. Ed. Engl.* **1995**, *34*, 2031–2033.
3. (a) Zylstra, G. J.; Gibson, D. T. *J. Biol. Chem.* **1989**, *264*, 14940–14946; (b) Vila, M. A.; Brovetto, M.; Gamenara, D.; Bracco, P.; Zinola, G.; Seoane, G.; Rodríguez, S.; Carrera, I. *J. Mol. Catal. B: Enzym.* **2013**, *96*, 14.
4. (a) Griffen, J.; Kenwright, S.; Abou-Shehada, S.; Wharry, S.; Moody, T.; Lewis, S. *Org. Chem. Front.* **2014**, *1*, 79–90; (b) Adams, D. R.; van Kempen, J.; Hudlicky, J. R.; Hudlicky, T. *Heterocycles* **2014**, *88*, 1255–1274; (c) Pilgrim, S.; Kociok-Kohn, G.; Lloyd, M. D.; Lewis, S. E. *Chem. Commun.* **2011**, 4799–4801; (d) Griffen, J. A.; Le Coz, A. M.; Kociok-Kohn, G.; Ali Khan, M.; Stewart, A. J. W.; Lewis, S. E. *Org. Biomol. Chem.* **2011**, *9*, 3920–3928; (e) Adams, D. R.; Aichinger, C.; Rinner, U.; Hudlicky, T. *Synlett* **2011**, 0725–0729; (f) Fischer, T. C. M.; Leisch, H. G.; Mihovilovic, M. D. *Montash Chem.* **2010**, *141*, 699–707; (g) Charest, M. G.;

Lerner, C. F.; Brubaker, J. D.; Siegel, D. R.; Myers, A. G. *Science* **2005**, *308*, 395–398; (h) Mihovilovic, M. D.; Leisch, H. G.; Mereiter, K. *Tetrahedron Lett.* **2004**, *45*, 7087–7090; (i) Myers, A. G.; Siegel, D. R.; Buzard, D. J.; Charest, M. G. *Org. Lett.* **2001**, *3*, 2923–2926; (j) Jenkins, G. N.; Ribbons, D. W.; Widdowoson, D. A.; Slawin, A. M. Z.; Williams, D. J. *J. Chem. Soc. Perkin Trans. 1* **1995**, 2647–2655; (k) Parker, M. H.; Maryanoff, B. E.; Reitz, A. B. *Synlett* **2004**, 2095–2098; (l) Ali Kahn, M.; Lowe, J. P.; Johnson, A. L.; Stewart, A. J. W.; Lewis, S. E. *Chem. Commun.* **2011**, 215–217; (m) Palframan, M. J.; Kociok-Kohn, G.; Lewis, S. E. *Org. Lett.* **2011**, *13*, 3150–3153; (n) Ali Kahn, M.; Mahon, M. F.; Lowe, J. P.; Stewart, A. J. W.; Lewis, S. E. *Chem.-Eur. J.* **2012**, *18*, 13480–13493.

5. (a) McKibben, B. P.; Barnosky, G. S.; Hudlicky, T. *Synlett* **1995**, 806–808; (b) Pittol, C. A.; Pryce, R. J.; Roberts, S. M.; Ryback, G.; Sik, V.; Williams, J. O. *J. Chem. Soc., Perkin Trans.* **1989**, *1*, 1160–1162.
6. Mahon, M. F.; Molloy, K.; Pittol, C. A.; Pryce, R. J.; Roberts, S. M.; Ryback, G.; Sik, V.; Williams, J. O.; Winders, J. A. *J. Chem. Soc., Perkin Trans.* **1991**, *1*, 1255–1263.
7. (a) Harrison, D. P.; Iovan, D. A.; Myers, W. H.; Sabat, M.; Wang, S.; Zottig, V. E.; Harman, W. D. *J. Am. Chem. Soc.* **2011**, *133*, 18378–18387; (b) Gillard, J. R.; Burnell, D. J. *J. Chem. Soc., Chem. Commun.* **1989**, 1439–1440.
8. Banwell, M. G.; Dupuche, J. R. *J. Chem. Soc., Chem. Commun.* **1996**, 869–870.
9. Hudlicky, T.; McKibben, B. P. *J. Chem. Soc., Perkin Trans.* **1994**, *1*, 485–486.
10. (a) Hudlicky, T.; Olivo, H. F. *J. Am. Chem. Soc.* **1992**, *114*, 9694–9696; (b) Hudlicky, T.; Olivo, H. F. *Tetrahedron Lett.* **1991**, *32*, 6077–6080; (c) Braun, H.; Burger, W.; Kresze, G.; Schmidtchen, F. P.; Vaerman, J. L.; Viehe, H. G. *Tetrahedron: Asymmetry* **1990**, *1*, 403–415.
11. (a) Hudlicky, T.; Luna, H.; Barbieri, G.; Kwart, L. D. *J. Am. Chem. Soc.* **1988**, *110*, 4735–4741; (b) Carless, H. A. J.; Oak, O. Z. *Tetrahedron Lett.* **1989**, *30*, 1719–1720; (c) Hudlicky, T.; Price, J. D.; Luna, H.; Andersen, C. M. *Synlett* **1990**, 309–310; (d) Hudlicky, T.; Luna, H.; Olivo, H.; Andersen, C.; Nugent, T.; Price, J. *J. Chem. Soc., Perkin Trans.* **1991**, *1*, 2907–2917.
12. Banwell, M.; Darmos, P.; McLeod, M. D.; Hockless, D. C. R. *Synlett* **1998**, 897–899.
13. Banwell, M. G.; Edwards, A. J.; Harfoot, G. J.; Jolliffe, K. A. *Tetrahedron* **2004**, *60*, 535–547.
14. Griffen, J. A.; White, J. C.; Kociok-Kohn, G.; Lloyd, M. D.; Wells, A.; Arnot, T. C.; Lewis, S. E. *Tetrahedron* **2013**, *69*, 5989–5997.
15. Palframan, M. J.; Kociok-Kohn, G.; Lewis, S. E. *Chem. Eur. J.* **2012**, *18*, 4766–4774.
16. (a) Heintzelman, G. R.; Meigh, I. R.; Mahajan, Y. R.; Weinreb, S. M. Diels–Alder Reactions of Imino Dienophiles. In *Organic Reactions*; John Wiley & Sons, Inc, 2004; (b) Johannsen, M.; Yao, S.; Graven, A.; Jorgensen, A. *Pure Appl. Chem.* **1998**, *70*, 1117–1122.
17. (a) Xu, G.; Lv, B.; Roberge, J. Y.; Xu, B.; Du, J.; Dong, J.; Chen, Y.; Peng, K.; Zhang, L.; Tang, X.; Feng, Y.; Xu, M.; Fu, W.; Zhang, W.; Zhu, L.; Deng, Z.; Sheng, Z.; Welihinda, A.; Sun, X. *J. Med. Chem.* **2014**, *57*, 1236–1251; (b) Nomura, S.; Sakamaki, S.; Hongu, M.; Kawanishi, E.; Koga, Y.; Sakamoto, T.; Yamamoto, Y.; Ueta, K.; Kimata, H.; Nakayama, K.; Tsuda-Tsukimoto, M. *J. Med. Chem.* **2010**, *53*, 6355–6360; (c) Horne, G.; Wilson, F. X.; Tinsley, J.; Williams, D. H.; Storer, R. *Drug Discovery Today* **2011**, *16*, 107–118; (d) Dragutan, I.; Dragutan, V.; Demonceau, A. *RSC Advances* **2012**, *2*, 719–736.
18. (a) Johnson, C. R.; Johns, B. A. *J. Org. Chem.* **1997**, *62*, 6046–6050; (b) Johns, B. A.; Pan, Y. T.; Elbein, A. D.; Johnson, C. R. *J. Am. Chem. Soc.* **1997**, *119*, 4856–4865.
19. Baillargé, M.; Le Goffic, F. *Synth. Commun.* **1987**, *17*, 1603–1606.
20. (a) Jung, M. E.; Shishido, K.; Light, L.; Davis, L. *Tetrahedron Lett.* **1981**, *22*, 4607–4610; (b) Yamazaki, H.; Horikawa, H.; Nishitani, T.; Iwasaki, T.; Nosaka, K.; Tamaki, H. *Chem. Pharm. Bull.* **1992**, *40*, 102–108; (c) Jäger, M.; Polborn, K.; Steglich, W. *Tetrahedron Lett.* **1995**, *36*, 861–864; (d) Gaitanopoulos, D. E.; Weinstock, J. *J. Heterocycl. Chem.* **1985**, *22*, 957–959.
21. Hudlicky, T.; Boros, E. E.; Olivo, H. F.; Merola, J. S. *J. Org. Chem.* **1992**, *57*, 1026–1028.
22. Karplus, M. *J. Am. Chem. Soc.* **1963**, *85*, 2870–2871.
23. Li, L.-C.; Jiang, J.-X.; Ren, J.; Pittman, C.; Zhu, H.-J. *Eur. J. Org. Chem.* **2006**, 1981–1990.
24. (a) Jones, G. A.; Shephard, M. J.; Paddon-Row, M. N.; Beno, B. R.; Houk, K. N.; Redmond, K.; Carpenter, B. K. *J. Am. Chem. Soc.* **1999**, *121*, 4334–4339; (b) Liu, J.; Niwayama, S.; You, Y.; Houk, K. N. *J. Org. Chem.* **1998**, *63*, 1064–1073; (c) Houk, K. N.; Li, Y.; Evanseck, J. D. *Angew. Chem., Int. Ed.* **1992**, *31*, 682–708.
25. (a) Domingo, L. R.; Jones, R. A.; Picher, M. T.; Sepulveda-Arques, J. *Tetrahedron* **1995**, *51*, 8739–8748; (b) Domingo, L. R.; Jones, R. A.; Picher, M. T.; Sepulveda-Arques, J. *J. Mol. Struct. (Theochem)* **1996**, *362*, 209–213; (c) Domingo, L. R.; Picher, M. T.; Andres, J.; Moliner, V.; Safont, V. S. *Tetrahedron* **1996**, *52*, 10693–10704; (d) Domingo, L. R.; Picher, M. T.; Andres, J.; Safont, V. S. *J. Org. Chem.* **1997**, *62*, 1775–1778; (e) Domingo, L. R.; Picher, M. T.; Zaragoza, R. J. *J. Org. Chem.* **1998**, *63*, 9183–9189; (f) Domingo, L. R.; Picher, M. T.; Aurell, M. J. *J. Phys. Chem. A.* **1999**, *103*, 11425–11430; (g) Domingo, L. R.; Aurell, M. J.; Perez, O. *Contreras, R.* **2003**, *68*, 3884–3890.
26. Fleming, I. *Molecular Orbitals and Organic Chemical Reactions*, student edition; John Wiley & Sons Ltd: United Kingdom, 2009.
27. Domingo, L. R.; Sáenz, J. A. *J. Biol. Chem.* **2009**, *7*, 3576–3583.
28. Hutner, S. H.; Provasoli, L.; Schatz, A.; Haskins, C. P. *Proc. Am. Phil. Soc.* **1950**, *94*, 152–170.
29. Baillargé, M.; Le Goffic, F. *Synthetic Commun.* **1987**, *17*, 1603–1606.
30. Hyperchem 7.5 for Windows Molecular Modeling System, H. H. Inc, 2002.
31. Koch, W.; Holthausen, M. C. *A Chemist's Guide to DFT*, 2nd ed; Wiley: New York, 2001.
32. Lee, C.; Yang, W.; Parr, R. G. *Phys. Rev. B.* **1988**, *37*, 785.
33. Frisch, M. J.; Trucks, G. W.; Schlegel, H. B.; Scuseria, G. E.; Robb, M. A.; Cheeseman, J. R.; Scalmani, G.; Barone, V.; Mennucci, B.; Petersson, G. A.; Nakatsuji, H.; Caricato, M.; Li, X.; Hratchian, H. P.; Izmaylov, A. F.; Bloino, J.; Zheng, G.; Sonnenberg, J. L.; Hada, M.; Ehara, M.; Toyota, K.; Fukuda, R.; Hasegawa, J.; Ishida, M.; Nakajima, T.; Honda, Y.; Kitao, O.; Nakai, H.; Vreven, T., ; Montgomery, J. A., Jr.; Peralta, J. E.; Ogliaro, F.; Bearpark, M.; Heyd, J. J.; Brothers, E.; Kudin, K. N.; Staroverov, V. N.; Kobayashi, R.; Normand, J.; Raghavachari, K.; Rendell, A.; Burant, J. C.; Iyengar, S. S.; Tomasi, J.; Cossi, M.; Rega, N.; Millam, J. M.; Klene, M.; Knox, J. E.; Cross, J. B.; Bakken, V.; Adamo, C.; Jaramillo, J.; Gomperts, R.; Stratmann, R. E.; Yazyev, O.; Austin, A. J.; Cammi, R.; Pomelli, C.; Ochterski, J. W.; Martin, R. L.; Morokuma, K.; Zakrzewski, V. G.; Voth, G. A.; Salvador, P.; Dannenberg, J. J.; Dapprich, S.; Daniels, A. D.; Farkas, O.; Foresman, J. B.; Ortiz, J. V.; Cioslowski, J.; Fox, D. J. *Gaussian 09, R. A.*; Gaussian, Inc.: Wallingford CT, 2009.
34. (a) Vijaya, R.; Narahari Sastry, G. *Journal of Molecular Structure (Theochem)* **2002**, *618*, 201–208; (b) Alves, C. N.; Romero, O. A. S.; da Silva, A. B. F. *Journal of Molecular Structure (Theochem)* **2001**, *535*, 165–169; (c) Biesemans, M.; Dalil, H.; Nguyen, L. T.; Haelterman, B.; Decadt, G.; Verpoort, F.; Willem, R.; Geerlings, P. *Tetrahedron* **2002**, *58*, 10447–10453; (d) Snezhana, M.; Bakalova, M.; FGil Santos, A. *J. Org. Chem.* **2004**, *69*, 8475–8481.
35. García, J. I.; Mayoral, J. A.; Salvatella, L. *Acc. Chem. Res.* **2000**, *33*, 658.
36. (a) Foster, J. P.; Weinhold, F. *J. Am. Chem. Soc.* **1980**, *102*, 7211–7218; (b) Reed, A. E.; Weinstock, R. B.; Weinhold, F. *J. Chem. Phys.* **1985**, *83*, 735–746; (c) Reed, A. E.; Weinhold, F. *J. Chem. Phys.* **1985**, *83*, 1736–1740.
37. Seeman, J. I. *J. Chem. Ed.* **1986**, *63*, 42–48.
38. Gupta, K.; Giri, S.; Chattaraj, P. K. *J. Phys. Org. Chem.* **2012**, *26*, 187–193.

Please cite this article in press as: Pazos, M.; et al. *Tetrahedron: Asymmetry* (2015), http://dx.doi.org/10.1016/j.tetasy.2015.10.015